ACS APPLIED MATERIALS & INTERFACES

Research Article

www.acsami.org

Modification and Patterning of Nanometer-Thin Poly(ethylene glycol) Films by Electron Irradiation

Nikolaus Meyerbröker and Michael Zharnikov*

Angewandte Physikalische Chemie, Universität Heidelberg, Im Neuenheimer Feld 253, 69120 Heidelberg, Germany

ABSTRACT: In this study, we analyzed the effect of electron irradiation on highly cross-linked and nanometer-thin poly(ethylene glycol) (PEG) films and, in combination with electron beam lithography (EBL), tested the possibility to prepare different patterns on their basis. Using several complementary spectroscopic techniques, we demonstrated that electron irradiation results in significant chemical modification and partial desorption of the PEG material. The initially well-defined films were progressively transformed in carbon-enriched and oxygen-depleted aliphatic layers with, presumably, still a high percentage of intermolecular cross-linking bonds. The modification of the films occurred very rapidly at low doses, slowed down at moderate doses, and exhibited a leveling off behavior at higher doses. On the basis of these results, we demonstrated the fabrication of wettability patterns and sculpturing complex 3D microstructures on the PEG basis. The swelling behavior of such morphological patterns was studied in detail, and it was shown that, in contrast to the pristine material, irradiated areas of the PEG films reveal an almost complete absence of the hydrogel-typical swelling behavior. The associated sealing of the irradiated areas allows a controlled deposition of objects dissolved in water, such as metal nanoparticles or fluorophores, into the surrounding, pristine areas, resulting in the formation of nanocomposite patterns. In contrast, due to the distinct protein-repelling properties of the PEG films, proteins are exclusively adsorbed onto the irradiated areas. This makes such films a suitable platform to prepare protein-affinity patterns in a protein-repelling background.

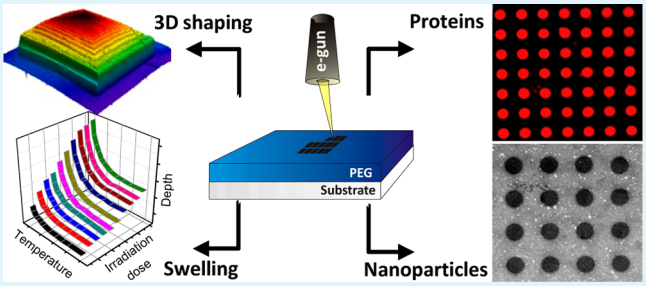

KEYWORDS: *poly(ethylene glycol), electron beam lithography, biocompatibility, hydrogel films, swelling, wetting properties*

1. INTRODUCTION

Poly(ethylene glycols) (PEGs) comprise an important class of synthetic polymers that resists the nonspecific adsorption of proteins, which makes them a valuable component for a variety of commercial products in such areas as cosmetics, drug delivery, tissue engineering, etc.[1] Along with bulk PEG materials, thin PEG films aroused considerable interest since they can be used for biocompatible surface coatings and as versatile model systems to investigate protein adsorption or cell adhesion.[2−4] Consequently, there is a large number of methods described in the literature to immobilize PEG onto different surfaces and prepare thin, biocompatible PEG films with thicknesses from a few to hundreds of nanometers.[2,5−12] A popular preparation route is the so-called "grafting-to" method, i.e. the attachment of appropriately functionalized PEG molecules to the substrate, directly or to an intermediate coupling moiety.[5,7,13−15] Another way is the "grafting-from" approach, i.e. the fabrication of PEG coatings by surface initiated polymerization (SIP).[11,16] Further, PEG films can be prepared by graft polymerization or copolymerization on different substrates which, in most cases, are specially functionalized to provide a chemical coupling to the PEG layer.[10,12,17] Alternatively, weakly surface-coupled PEG films can be prepared; they can be, if necessary, separated from the substrate and used as membranes.[18]

Along with the fabrication of PEG films, their modification by physical tools is also of importance, both in context of controlled protein adhesion and in view of lithographic applications. To this end, exposure of oligo(ethylene glycol) (OEG) terminated self-assembled monolayers (SAMs) on noble metal substrates[19,20] as well as thicker, polymer-like PEG films to ultraviolet (UV) light was investigated in detail.[21,22] In the case of SAMs, the exposure to UV light resulted in the damage and photooxidation of the OEG chains and thiolate headgroups, which can be used for controlled tuning of protein-repelling properties or UV-promoted exchange reaction with a molecule bearing a receptor for specific protein attachment.[20] In the case of polymer-like films, damage and photooxidation of the PEG chains were observed as well, with the film becoming significantly thinner and losing its protein-repelling properties in the course of UV treatment.[22] In combination with lithographic techniques, both SAMs and PEG films were used as templates for protein patterns; these templates comprised the UV-treated, protein-adhering areas and the pristine, biocompatible OEG/PEG matrix.[20,22]

Received: March 18, 2013
Accepted: May 2, 2013
Published: May 2, 2013

   dx.doi.org/10.1021/am400991h | *ACS Appl. Mater. Interfaces* 2013, 5, 5129−5138

Alternatively to UV light, modification of OEG- or PEG-based films can be performed by electrons, resulting, among other effects, in decomposition of the OEG/PEG moieties and gradual loss of protein-repelling properties.[23] Similar to the case of UV light, this behavior could be used for the preparation of mixed monolayers and fabrication of protein-affinity templates on the micro- and nanoscale.[23−26] However, such experiments have been discussed in the literature only for OEG terminated SAMs or relatively thin films, comprised of PEGs attached covalently to a silicon substrate.[23−26] It would be then interesting to investigate the effect of electron exposure in the case of polymer-like PEG films which possess a variety of interesting and useful properties along with their inertness to proteins.

Here we present the results of such experiments. As a model system, we used highly cross-linked, hydrogel-like PEG films which were described by us recently.[27] These films can be easily fabricated in a broad thickness range (4−100 nm) by thermo-activated, intermolecular cross-linking of epoxy and amine-terminated STAR-PEGs (Figure 1) and represent a promising

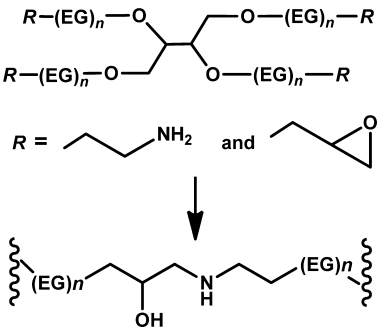

Figure 1. Chemical structure of amine- and epoxy-terminated, STAR-PEG compounds and a cross-linking unit after the reaction of the amine and epoxy groups.

alternative to the commonly used films of PEG acrylates, which are cross-linked photochemically by UV exposure, frequently with the addition of an initiator.[12,17] In our case, neither UV treatment nor initiator is necessary, along with a broad flexibility in terms of the substrate, which can be chosen arbitrarily and does not require any special treatment or activation.

In this study, the effect of electron irradiation on the chemical composition, protein-repelling properties, wetting properties, and the swelling behavior of the PEG films is analyzed in detail. To this end, we applied a variety of complementary experimental techniques as described in the next section. Along with the characterization of the homogeneous PEG films, we used them as a flexible platform for micro- and nanofabrication, preparing different patterns by electron beam lithography (EBL).

2. EXPERIMENTAL SECTION

Preparation of the PEG Films. The preparation procedure is illustrated schematically in Figure 1 and described in detail elsewhere.[27] In brief, epoxy- and amino-terminated, four-arm polyethylene glycols with M_N = 2000 g/mol (Creative PEGWorks, USA) were separately dissolved in chloroform with concentrations between 0.75 and 30 mg/mL and spin-coated as an equally concentrated 1:1 mixture on a 100 nm polycrystalline Au(111) substrate (Georg-Albert-PVD, Germany). Cross-linking of the PEG components was performed by gentle heating at 80 °C under argon atmosphere for 6 h, followed by ultrasonication or rinsing.

Electron Irradiation and Patterning. To monitor the effect of electron irradiation, the PEG films were irradiated homogenously by a flood gun (FG20, Specs, Germany) under ultrahigh vacuum (UHV) conditions (residual pressure <10^{-8} mbar). The electron energy was set to 50 eV, and the dose was calibrated by a Faraday cup. Simple lithographic patterns were fabricated in proximity printing geometry using either a macroscopic grid or a micrometer-size TEM grid (Quantfoil, R2/4) as a mask. For complex lithographic patterns, we used an EBL writer consisting of a LEO 1530 Gemini scanning electron microscope (SEM) and a special lithographic unit (Raith Elphy Quantum). The patterning was performed under high vacuum conditions (residual pressure <10^{-5} mbar). The energy of the electron beam was set to 3.0 keV, and the dose was calibrated by a Faraday cup. In some selected cases, dwell time and step size for the writing were set manually to avoid an over- or underexposure.

Note that not the entire film was affected in the electron beam modification process at the same time. The effective depth of modification depended on the kinetic energy of the primary electrons and, based on the attenuation length for the PEG films,[27] could be roughly estimated at ca. 3 nm for the 50 eV electrons and ca. 37 nm for 3 keV electrons. So, at least in the case of 50 eV electrons, the film was modified from the top down, in a layer-by-layer fashion.

Spectroscopic Characterization. Irradiation-induced changes in the chemical composition and thickness of the PEG films were monitored by X-ray photoelectron spectroscopy (XPS). To avoid any kind of contamination and to exclude successive oxidation, the measurements were carried out in situ, in the same UHV system as the electron irradiation. The XPS spectrometer (MAX200, Leybold-Heraeus) was equipped with a Mg Kα X-ray source (1253.6 eV; 200 W) and a hemispherical analyzer. The recorded spectra were normalized to the transmissions function of the spectrometer, and the binding energy (BE) scale was referenced to the Au $4f_{7/2}$ peak of clean gold at 84.0 eV.[28] The spectra were fitted by symmetric Voigt functions using a Shirley-type background. The effective thicknesses of the PEG films were evaluated using the attenuation of the Au 4f signal from the substrate; the required attenuation length of 5.0 (±0.3) nm was obtained from the calibration measurements on a series of PEG-films with different thicknesses which were determined by ellipsometry assuming a standard Cauchy layer model for polymers.[27]

Spectroscopic Characterization at Synchrotron. For a few selected samples, irradiation-induced changes in the chemical composition were monitored by synchrotron-based XPS and near-edge X-ray fine structure (NEXAFS) spectroscopy. These experiments were performed ex situ; i.e. the irradiated PEG films were exposed to ambience prior to the measurements. The experiments were performed at the bending magnet beamline D1011 at the MAX II storage ring of the MAX-lab synchrotron radiation facility in Lund, Sweden.

The XPS spectra were collected using normal emission geometry at a photon energy of 580 eV. The energy resolution was ∼0.2 eV.

The acquisition of the NEXAFS spectra was carried out at the C K-edge in the partial electron yield mode with a retarding voltage of −150 V. Linear polarized synchrotron light with a polarization factor of 95% was used. The incidence angle was kept at 55° to exclude the orientation effects.[29] The energy resolution was ∼100 meV. Raw spectra were normalized to the incident photon flux by division through a spectrum of a clean, freshly sputtered gold sample. The photon energy scale was referenced to the pronounced π^* resonance of highly oriented pyrolytic graphite at 285.38 eV.[30]

Topography and Swelling Properties. The lithographically created topographic patterns were characterized by atomic force microscopy (AFM) using a Dimension 3100 microscope (Digital Instruments) with a Nanoscope IIIa controller (Veeco Instruments). The measurements were performed under ambient conditions, in the tapping mode. To monitor the swelling properties, the films were placed on a home-built, computer-controlled Peltier plate, which allowed, in a controlled fashion, the temperature of the films and, consequently, the relative humidity experienced by them to vary. To

ensure reliable results, all reference measurements were carried out under well-defined conditions in terms of temperature (20 ± 1 °C) and relative humidity (22 ± 1%).

Biocompatibility. For monitoring the effect of electron exposure on the biocompatibility, the PEG films were patterned by EBL, immersed into a filtered, PBS-buffered solution of red-fluorescent AlexaFluor647 fibrinogen conjugate (Invitrogen; 0.25 mg/mL; 60 min) under ambient conditions, and subsequently rinsed with copious amounts of Milli-Q water. The results of the protein adsorption experiments were monitored by fluorescence microscopy (FM). For control experiments, EBL patterned films were immersed into an aqueous solution (5% ethanol) of fluorescein (1 mg/mL) for 6 h, gently rinsed with water, and investigated by FM.

PEG-Based Composites. PEG/gold nanoparticle (AuNPs) composite patterns were prepared on the basis of the PEG films. Adsorption of AuNPs was carried out by immersion of the EBL-patterned PEG films into an aqueous solution of freshly prepared, citrate-stabilized AuNPs for 12 h, followed by extensive rinsing with water and drying in a nitrogen stream. The citrate-stabilized AuNPs with a diameter of ~20 nm were prepared by the reduction of $AuCl_3$ according to well-established protocols.[31] In brief, 50 mg of $HAuCl_4 \cdot 3H_2O$ were dissolved in 150 mL of water and heated to boiling. Under vigorous stirring, 150 mg of sodium citrate, dissolved in 15 mL of water, was added. The color changed from initially yellow to deep purple, indicating the formation of colloidal gold particles. The patterns were characterized using a LEO 1530 Gemini SEM under high vacuum conditions.

3. RESULTS AND DISCUSSION

3.1. Desorption and Changes in the Chemical Composition.

XPS is the most common technique to obtain information about the chemical composition of surfaces and thin films. Figure 2a shows exemplarily the survey spectrum of a pristine 40 nm PEG film. It is dominated by the characteristic O 1s peak of oxygen at ~533 eV and the C 1s emission of carbon at ~286 eV, both originating from the PEG film. Due to the self-attenuation of these signals,[32] the spectra for the PEG films with other thicknesses differ only slightly. For the films with thicknesses below 30 nm, the Au 4f signal from the gold substrate also becomes visible.

A closer examination of the C 1s spectrum reveals that it consists of two emissions as shown in Figure 2b, bottom. The high energy peak at 286.4 eV (highlighted gray) is characteristic of carbon atoms in the ether groups of PEG, while the significantly weaker, low energy peak at 284.4 eV stems presumably from the carbon atoms beyond the PEG chains of the STAR-PEG moieties (Figure 1).[33]

After exposure of the PEG films to 50 eV electrons, the C 1s spectrum undergoes significant changes. Even at a small dose of 5 mC/cm^2, the high energy peak decreases in favor of the low energy one (Figure 2b, middle), which becomes the dominant feature with the progressive irradiation (Figure 2b, top). Simultaneously, the intensity of the O 1s signal decreases (Figure 2c), while the intensity of the Au 4f signal from the substrate increases, and it gets visible even for the thick PEG films (Figure 2d). The observed evolution of the XPS spectra suggests a noticeable extent of irradiation-induced desorption as well as significant modifications in the chemical composition of the residual PEG films.

This transformation is accompanied by the changes in the positions and widths of the photoemission peaks as shown in Figure 3 where these changes are plotted as functions of irradiation dose. The full widths at half-maximum (fwhm) of both C 1s and O 1s emissions increased continuously and in a similar fashion with progressive irradiation, exhibiting a leveling off behavior at high doses as shown in Figure 3a and b. The observed broadening suggests continuous deterioration of the chemical homogeneity within the film in the course of the irradiation treatment.

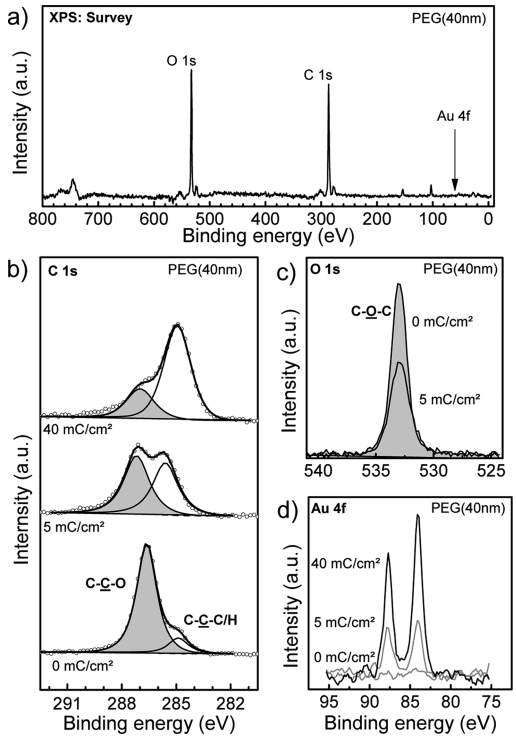

Figure 2. XPS spectra of a PEG film with an initial thickness of 40 nm: (a) survey spectrum of the pristine film; C 1s (b), O 1s (c), and Au 4f (d) spectra of the pristine and irradiated films. The C 1s spectra are decomposed into two individual emissions. The emissions assigned to the pristine and modified ether groups are shadowed gray in b and c. The irradiation doses are given at the respective spectra.

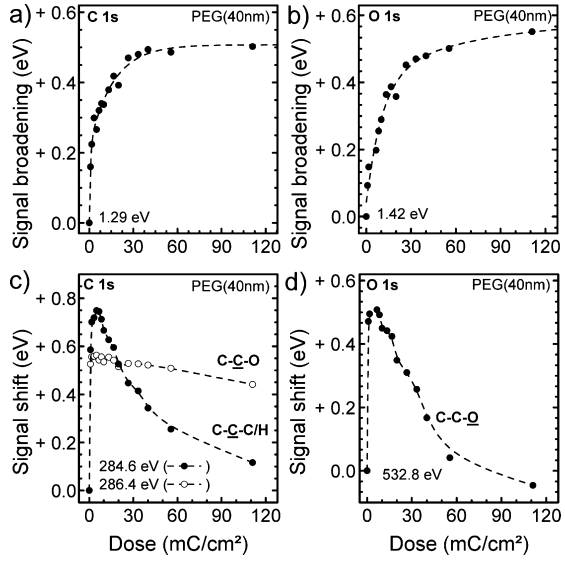

Figure 3. Parameters of the C 1s and O 1s emissions as functions of irradiation dose for a 40 nm PEG film. (a,b) fwhm increase for the C 1s (a) and O 1s (b) emissions; (c,d) binding energy shifts for the C 1s (c) and O 1s (d) emissions. In c, the data for both low energy (filled circles) and high energy (open circles) peaks are presented.

dx.doi.org/10.1021/am400991h | ACS Appl. Mater. Interfaces 2013, 5, 5129−5138

More unusual is the dose-dependent behavior of the C 1s and O 1s peak positions shown in Figure 3c and d. The positions shift abruptly by 0.5−0.8 eV to the higher binding energies at low irradiation doses (<8 mC/cm^2) and move back, toward the lower energies, at higher doses. The behavior of the low energy C 1s emission mimics that of the O 1s peak, while the high energy C 1s emission shows a smaller shift at the low doses and much slower recovery at higher doses. Note that the shift behavior is nearly independent of the film thickness, which means that it solely reflects chemical transformation of the PEG films upon the irradiation.

The extent of the observed changes suggests that this transformation is quite severe and most rapid at small doses, which agrees with the tremendous changes in the XPS spectra in this dose range (Figure 2). However, the observed behavior cannot be associated with some certain chemical changes since it cannot be explained within the standard concept of the chemical shift. The C 1s and O 1s emissions are displaced very similarly and in the same direction, whereas shifts in the opposite directions are expected in the standard situation. The most probable reason for the observed shifts are the charging effects which are observed quite frequently for nonconductive polymer samples during the XPS analysis.[34] The extent and character of charging can vary significantly depending on the exact chemical composition of the PEG film, which changes in the course of the irradiation.

Along with the positions and FWHMs of the photoemission peaks, their intensity can be monitored. In particular, the intensity of the Au 4f emission can be used to calculate the film thickness. The respective results are presented in Figure 4a for the PEG films with initial thicknesses of 15 and 40 nm. Both films exhibit similar behavior in the course of the irradiation treatment, with some minor differences presumably explained by the fact that the Au 4f signal was not initially perceptible for the 40 nm film, and we had to use the ellipsometry-derived thickness value for this particular case. The observed similarity is most likely related to the limited effective penetration depth of 50 eV electrons, which is only a couple of nanometers.[35] Therefore, the total film thickness is of minor importance only, at least at the initial stage of the irradiation treatment. The most significant loss of the film thickness occurred at small doses. In particular, almost the half of the 15 nm film was lost after the irradiation with a dose of 10 mC/cm^2. At higher doses, saturation-like behavior is observed and the film exhibits a continuous decrease in the thickness with increasing dose, even though with a smaller rate as compared to the low doses. An explanation for this dose-dependent degeneration process is given below.

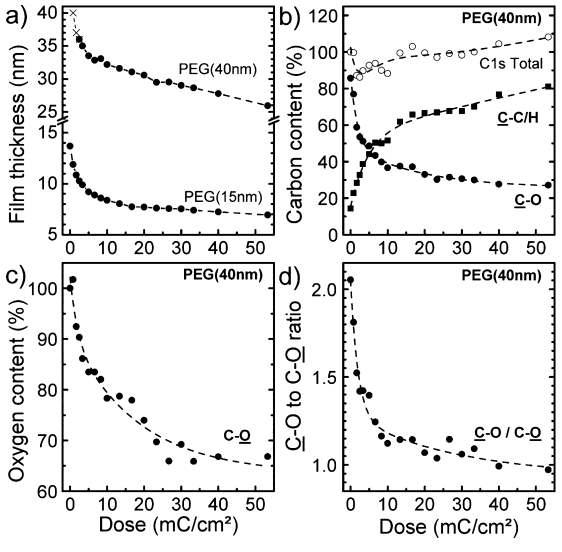

Figure 4. XPS-derived parameters for a PEG film with an initial thickness of 40 nm as functions of irradiation dose: (a) film thickness, along with the analogous data for a PEG film with an initial thickness of 15 nm; (b) intensities of the high (filled circles) and low (filled squares) energy C 1s emissions as well as the total C 1s intensity (open circles); (c) relative intensity of the O 1s emission; (d) carbon to oxygen ratio, with only the high energy peak taken into account in the case of carbon.

Whereas the reduction of the film thickness reflects irradiation-induced desorption, chemical changes in the residual film can be monitored using the intensities of the C 1s and O 1s emissions which are presented in Figure 3b and c as functions of the irradiation dose. The total carbon intensity increases slightly with increasing dose (Figure 4b) as a consequence of the strong decrease in the oxygen content down to 65% of its initial value (Figure 4c), which leads to a reduced self-attenuation of the C 1s signal. This also means that much more oxygen than carbon is lost during the irradiation process.

But also carbon itself undergoes a substantial rearrangement. Initially, the relative intensity of the high energy C 1s emission assigned to the ether species in the pristine PEG films is ∼88% of the total C 1s intensity. After the irradiation with a dose of 10 mC/cm^2, this value falls to ∼40% and, with further exposure, below 22%. Simultaneously, the relative intensity of the low energy C 1s emission, assigned to the aliphatic carbon, increases from initially ∼12% to ∼78% at high irradiation doses. These intensity values correspond to the fractions of the respective species since the attenuation of both C 1s peaks occurred in a similar way.

Using the tabulated sensitivity factors, relative concentration of the individual species in the PEG films can be calculated on the basis of the XPS data.[28,35] In particular, relative concentration of the oxygen-bound carbon and oxygen can be evaluated on the basis of the weighted intensity ratio of the high-energy C 1s peak and O 1s emission. The oxygen-bound carbon is a constituent of the ether groups for the pristine PEG films but changes its chemical identity in the course of irradiation. Significantly, the pristine PEG films exhibited a stoichiometric ether carbon to oxygen ratio close to the ideal value of 2:1 (Figure 4d). This confirms that the high energy C 1s emission and O 1s peak in the respective spectra are indeed exclusively attributed to the PEG material. However, upon irradiation, the oxygen-bound carbon to oxygen ratio decreases progressively and saturates at a value close to 1 at high doses (Figure 4d). Hence, on the average, every oxygen atom is bound to only one carbon atom in the heavily irradiated PEG films. Such a stoichiometric ratio does not match that of PEGs, so that the oxygen must be likely present as hydroxy groups, especially because no carbonyl species at higher binding energies are detectable in the C 1s XPS spectra.

It is known that electron-induced cleavage of a C−C bond is promoted by an oxygen in the α-position to it.[36] This is exactly the situation occurring for PEGs, with oxygen playing the role of heteroatom, which explains the high sensitivity of PEG material toward electron irradiation. The electron beam cleaves the chemical bonds within the PEG films, the fragments of which desorb into the vacuum, mediating the observed

thickness reduction. The remaining fragments rearrange immediately to a new structure with a higher content of C−C bonds, which is in agreement with the increase of the aliphatic carbon signal. Such a structure, which presumably includes extensive intermolecular cross-linking,[25] is more stable against electron irradiation as compared to the pristine PEG films because carbon is no longer bound to oxygen. This explains the increased stability of the film with progressing electron irradiation, which manifests itself in a two-phase-like degeneration process in Figure 4a.

In addition to the C−C bonds, a C═C motif appears as well, which is typical of irradiated aliphatic SAMs.[37,38] In Figure 5a,

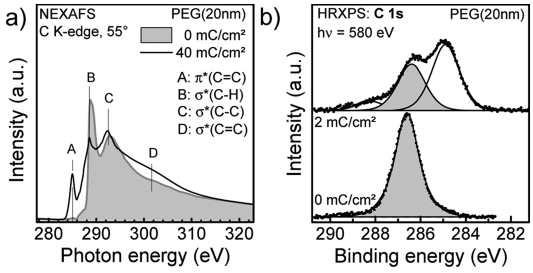

Figure 5. (a) C K-edge NEXAFS spectra of the pristine (gray shaded) and irradiated (40 mC/cm^2) PEG films (20 nm). The characteristic absorption resonances are marked. (b) Synchrotron-based C 1s XPS spectra of the pristine and irradiated (2 mC/cm^2) PEG films (20 nm). The latter spectrum is decomposed in individual peaks. The high energy peak is gray shaded.

C K-edge NEXAFS spectra of the pristine and heavily irradiated (40 mC/cm^2) 20 nm PEG films are presented. The spectrum of the pristine film exhibits characteristic absorption resonances of the OEG and PEG moieties at 288.9 eV (B) and 292.4 eV (C) assigned to the C−H orbitals of OEG/PEG and to the σ^* orbitals of C−C and C−O bonds, respectively.[39−41] These resonances disappear (B) or shift significantly (C) upon the irradiation, assuming, in accordance with the XPS data, severe modification of the PEG film. In addition, a new resonance at 285.0 eV (A) appears and can be clearly assigned to C═C bonds,[29] which evidence their creation in the course of electron irradiation. The presence of these bonds, also as intermolecular cross-links, is an additional factor explaining the stability of the irradiated films.

The C K-edge NEXAFS spectra in Figure 5a are complemented by the synchrotron-based C 1s XPS spectra of the pristine and irradiated (2 mC/cm^2) 20 nm PEG films in Figure 5b. These spectra were acquired at a lower photon energy than those presented in Figure 2, so that the respective sampling depth is smaller and the spectra are mostly characteristic of the topmost part of the PEG films. Significantly, the spectrum of the pristine film exhibits only the high energy peak, whereas the low energy feature is only visible as a small shoulder. This implies a preferable segregation of the PEG chains at the PEG-ambience interface, which is certainly of advantage for the protein-repelling behavior of these films. The spectra of the irradiated film look similar to those in Figure 2 with the only difference that there is an additional feature at ∼288.5 eV which is presumably assigned to oxygen contamination since the samples were exposed to ambience before the measurements.

3.2. Influence of Irradiation on Material Loss. The significant extent of desorption (i.e., material loss) from the PEG films upon electron irradiation could be visualized and monitored in detail using a combination of EBL and AFM. This is demonstrated by the example of a 65 nm PEG film which was subjected to the successive writing of the cocentered squares of decreasing size, so that the total dose increased inward in a step-like manner. The color-coded AFM image of the resulting dip pattern is shown in Figure 6a while the inverse replica of

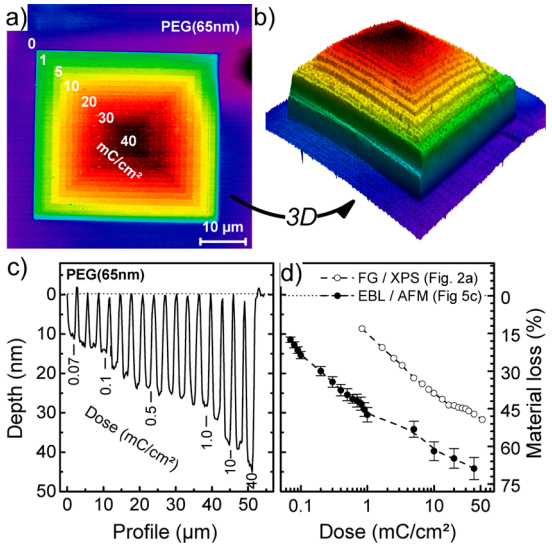

Figure 6. The results of the EBL experiments on a 65 nm PEG film. (a) Color-coded AFM image of a pattern consisting of the successively written, cocentered squares of decreasing size; the total doses corresponding to the different areas of the pattern are given in several places. (b) Inverse replica (3D) of the image in a. (c) AFM depth profile across the array of the circular pits written with the increasing doses as marked in the plot. (d) Relative material loss as a function of irradiation dose (filled circles), along with the analogous curve obtained on the basis of the XPS data (open circles).

this image is presented in Figure 6b in 3D fashion. This replica represents a step-like, squared pyramid, with the individual steps being well distinguishable, especially for the small total doses. According to the replica, the extent of desorption increases (nonlinearly) from the outside to the center of the pattern, i.e. with the increasing total dose, in full agreement with the XPS data (see previous section). This behavior allows creating 3D micro- and nanostructures of arbitrary shape in the PEG matrix by adjusting the dose for each particular area. The inverse pyramid presented in Figure 6b is a representative example of such a microstructure.

To describe the relation between the dose and extent of desorption more quantitatively, an array of circular pits was written into the 65 nm PEG film with doses between 0.1 and 40 mC/cm^2. The respective AFM depth profile across the array is shown in Figure 6c. Again, the strong influence of the dose on the extent of desorption, reflected by the depths of the individual pits, is well recognizable; the respective material loss is plotted as a function of the dose in Figure 6d (filled circles). The nonlinear character of the relation between the dose and material loss is compensated by the semilogarithmic character of the plot, resulting in the close-to-linear curve. In accordance with Figure 3a and b, the material loss is especially strong at low doses, achieving almost 50% at a dose of only 1 mC/cm^2. A further increase in the dose leads to a smaller material loss

dx.doi.org/10.1021/am400991h | ACS Appl. Mater. Interfaces 2013, 5, 5129−5138

which achieves ~75% at the maximum applied dose (40 mC/cm^2).

Along with the AFM derived material losses, analogous values obtained from the XPS data (see previous section) are shown additionally in Figure 6d (open circles). Although the trend of both curves is similar, the absolute values of the material loss differ significantly. This is related to the different energies of electrons used in the EBL (3 keV) and XPS (50 eV) experiments. The material loss is more extensive for the 3 keV electrons as compared to the 50 eV ones provided by the flood gun (FG). This can be explained by an about 10-fold penetration depth[35] and a higher efficiency[42] of the higher energy electrons.

3.3. Influence of Irradiation on the Wetting Properties. Interaction of surfaces with liquids depends on their chemical composition and morphology, so that, in view of the results presented in the previous sections, wetting properties of the PEG films should be strongly affected by electron irradiation. The static water contact angles (CA) for both pristine and irradiated (10 mC/cm^2; 50 eV) PEG films are plotted in Figure 7a as functions of the film thickness. The CA

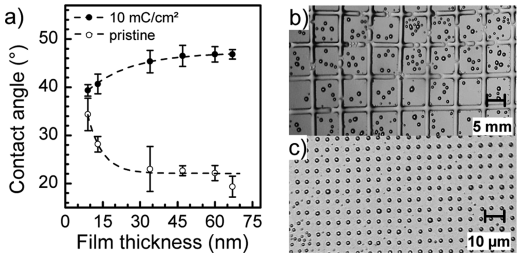

Figure 7. (a) Static contact angles of the pristine and irradiated (10 mC/cm^2; 50 eV) PEG films as functions of the film thickness (open and filled circles, respectively). (b,c) Optical microscopy images of the hydrophilicity patterns written in the PEG matrix by proximity printing using the stencil masks with either macroscopic (b) or microscopic (c) openings. The images were taken after the cooling-driven moisture condensation.

values for the pristine films decrease gradually with increasing thickness from 34° for a 10 nm film to ~20° for 25–30 nm films and exhibit leveling off character at higher thicknesses. This behavior can be tentatively explained by the variable degree of cross-linking for the thinner films; the CA decrease at low thicknesses correlates well with the behavior of the swelling factor which, in the given case, is a fingerprint parameter for the extent of cross-linking.[27] Note that the occurrence of swelling made it quite difficult to measure the contact angles of the pristine PEG films by the used sessile drop method. Because of the swelling, static contact angles of water dropped down to ~10° within a minute. Reasonably reliable and reproducible results could only be achieved when the contact angles were determined within a shorter time, which was after exactly 10 s in our case.

In contrast to the pristine films, the contact angles of the irradiated films remained constant over time and were considerably higher than those obtained for the respective nonirradiated films. This behavior is in good agreement with the XPS results (see section 3.1). The irradiated films underwent severe chemical transformation as compared to the pristine ones; they became enriched with aliphatic carbon, getting, therefore, considerably more hydrophobic and losing the typical swelling properties of the PEG hydrogels.

The effect of electron irradiation on the wetting properties can be used to write hydrophobic patterns into the hydrophilic PEG matrix by EBL. As representative examples, we prepared several such patterns using proximity printing geometry and a flood gun as the primary source of electrons. In the first case, we used a macroscopic stencil mask with 5 mm square holes. The optical microscopy image of the resulting structure is shown in Figure 7b illustrating the effect of the reduced hydrophilicity of the irradiated areas. When the pattern placed on a Peltier plate was cooled down to 1 °C under ambient conditions, moisture was condensed predominantly on the nonirradiated, hydrophilic areas. In contrast, when the PEG film was irradiated though a microscopic stencil mask with an opening diameter of only 2 μm (TEM grid Quantifoil R2/2), a reversed condensation pattern was obtained, with the moisture deposited only on the irradiated spots (Figure 7c). In this case, the condensation was presumably governed by the minimization of the surface tension and increased surface roughness in the irradiated areas.

3.4. Influence of Irradiation on the Swelling Behavior. The results presented in the previous section suggest that the swelling behavior of the PEG films can be affected by electron irradiation. To study this effect in detail, the films were patterned by EBL and then placed on a temperature-controlled Peltier plate, which allowed us to change the relative humidity above the film surface and, consequently, to control precisely the amount of water accumulated by the film. The degree of swelling over the fabricated patterns was monitored by AFM. Note that no swelling occurred at room temperature,[27] so that the respective data can be taken as a reference.

Figure 8a shows a 3D AFM image of a circular pit array written in a 100 nm PEG film with successively increasing doses

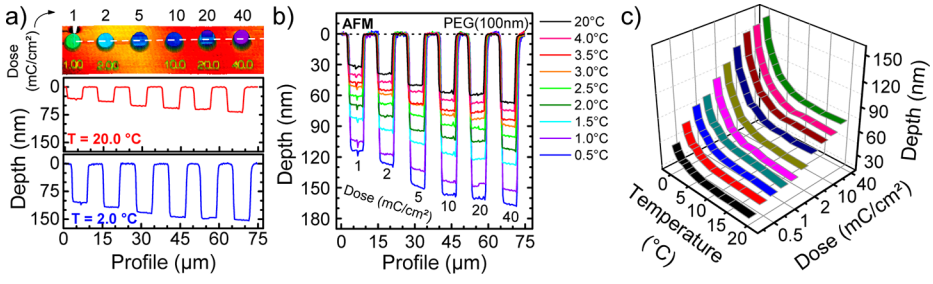

Figure 8. Influence of irradiation on the swelling properties of the PEG films: (a) AFM image (3D) of a circular pit array written in a 100 nm PEG film with doses of 1, 2, 5, 10, 20, and 40 mC/cm^2 (top panel), along with the corresponding height profiles across the array, recorded at 20 °C (middle panel) and 2 °C (bottom panel). (b) Height profiles measured across the same pit array taken at a variety of different temperatures between 0.5 and 20 °C. (c) 3D diagram summarizing the dependence of the pit depth on the temperature and dose.

dx.doi.org/10.1021/am400991h | ACS Appl. Mater. Interfaces 2013, 5, 5129–5138

Table 1. Parameters *A*, *B*, *A*+*B*, and *k* from eq 1 for a 100 nm PEG Film Exposed to Different Irradiation Doses

dose (mC/cm^2)	0.1	0.3	0.5	0.8	1	2	5	10	20	40
A (nm)	19	28	31	31	35	41	52	59	62	68
B(nm)	34	47	60	70	79	88	92	98	100	98
A+*B* (nm)	52	75	91	102	114	128	144	157	162	165
k(°C)	2.6	2.3	2.4	2.6	2.6	2.5	2.5	2.4	2.5	2.6

in a range of 1−40 mC/cm^2, along with the corresponding height profiles across the array, recorded at 20 and 2 °C. A distinctly larger depth of the pits at the lower temperature is well visible and unequivocally attributed to the swelling of the PEG material. However, it is not clear to what extent the irradiated areas participate in this process.

Figure 8b presents the height profiles measured across the same pit array at a variety of different temperatures between 0.5 and 20 °C. One can see that the swelling of the film is most efficient at temperatures below 4 °C. This can be emphasized when summarizing the dependence of the pit depth on the temperature and dose in one 3D diagram which is shown in Figure 8c. Analysis of this diagram suggests that for a given dose *D* there is a relationship between the depth and temperature, which can be described by a phenomenological equation

$$d(T) = A + B\cdot\exp(-T/k) \quad (1)$$

Herein, $d(T)$ is the pit depth in nm, *T* is the temperature in °C, and *A*, *B*, and *k* are the parameters which have a real physical meaning. *A* indicates the pit depth at room temperature, i.e. in the nonswollen state, whereas *B* represents the maximum additional depth as a result of the swelling at low temperature. Consequently, *A*+*B* is the maximum reachable total depth. Finally, the reciprocal value of *k* can be interpreted as a sensitivity coefficient which indicates how strong the system swells at temperature changes. The derived values of *A*, *B*, *A*+*B*, and *k* for doses between 0.1 and 40 mC/cm^2 are compiled in Table 1. The parameters *A* and *B* in this table look strongly dose-dependent while *k* changes only slightly, being close to a value of ∼2.5 (±0.1) °C.

To monitor this behavior in detail, we plotted *A*, *B*, and *k* as functions of the dose in Figure 9a and b. It occurred that the curves for *A* and *B* as well as the analogous curve for *A*+*B* (not shown) can be described by a general phenomenological equation (exemplarily for *A*)

$$A(D) = V_A\cdot D^n/(q^n + D^n) \quad (2)$$

where *V*, *q*, and *n* are the fitting parameters. These parameters for the cases of *A*, *B*, and *A*+*B* are compiled in Table 2, while their meaning is illustrated in Figure 9c. *V* has a real physical meaning in the case of *A*, specifying the pit depth *d* in the nonswollen state. V_A has a value of 98 nm, which is almost exactly the ellipsometric thickness of the pristine 100 nm PEG film. Consequently, V_A can be interpreted as the pit depth for the infinite dose, corresponding to the complete removal of the PEG film in the nonswollen state (Figure 9c, left panel). Accordingly, for parameter *B*, which describes the maximum *additional* depth of the pits due to the swelling, V_B is this depth limit for large doses in the swollen state (Figure 9c, right panel). Interestingly, *B* is rising sharply already for small doses and finally reaches its maximum depth V_B = 101 nm already at 10 mC/cm^2 (Figure 9a), which means that the additional depth becomes independent of the dose. This can be explained assuming that only the pristine PEG surrounding is able to swell, whereas the irradiated areas lose this capacity almost completely at doses higher than 10 mC/cm^2. At the lower doses, a successive loss of the swelling capacity occurs in the course of irradiation. For example, just a dose of 4 mC/cm^2 is enough to suppress the swelling by more than 90%.

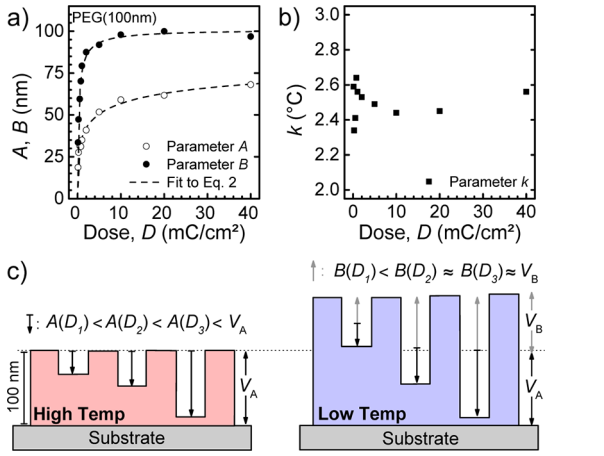

Figure 9. (a,b) Parameters *A* and *B* (a) and *k* (b) from eq 1 as functions of irradiation dose. The curves for *A* and *B* are fitted in accordance with eq 2. (c) Schematic drawings illustrating the physical meaning of the parameters used in eqs 1 and 2. Three pits corresponding to consequently increasing doses (D_1, D_2, and D_3) are shown in the nonswollen (left panel) and swollen (right panel) states.

Table 2. Parameters *V*, *q*, and *n* from eq 2 for the Cases of *A*, *B*, and *A*+*B*[a]

parameter	*V* (nm)	*q*	*n*	q^n
A (nm)	98 (1)	4.1	0.38	1.71
B (nm)	101 (2)	0.27	0.84	0.33
A+*B* (nm)	178 (2)	0.41	0.62	0.58

[a]The value for q^n is given as well.

Similar conclusions can be derived considering the values of the parameter *q* for *A* and *B* in Table 2. The smaller q_B is, the less the exposed regions are able to swell, so that the small value of q_B as compared to q_A manifests the proneness of the PEG films to irradiation-induced loss of hydrogel-like properties.

As an additional test for the reliability of the above analysis, one can use eq 2 and the respective parameters from Table 2 to evaluate the thickness and the swelling ratio of the pristine PEG films. The film thickness of 98 nm defined on the basis of V_A confirms the results of the ellipsometric measurements, while the swelling ratio, defined as $(V_A+V_B)/V_A$, is calculated to ∼2, which is in excellent agreement with the value given by ellipsometry for the 100 nm PEG film.[27]

3.5. Influence of Irradiation on the Adsorption of Proteins, Dyes, and Nanoparticles. Protein-repelling is the most important feature of OEG and PEG materials[1,43] as well as the PEG films of this study, in particular.[27] However, as reported in the literature,[15,23,25,26] OEG and PEG terminated

films become prone to the nonspecific protein absorption after their exposure to ionizing radiation. Using EBL, one can then write a protein affinity pattern in a protein repelling matrix.

Similar experiments were performed with the PEG films of this study. An array of circular structures with 5 μm diameter was generated by EBL (proximity printing; 3 keV; 10 mC/cm^2) in a 50 nm PEG film. Subsequently, the sample was incubated into a solution of fluorescently labeled fibrinogen and examined under a fluorescence microscope. The fluorescence microscopy (FM) image is shown in Figure 10a. As expected, the fibrinogen

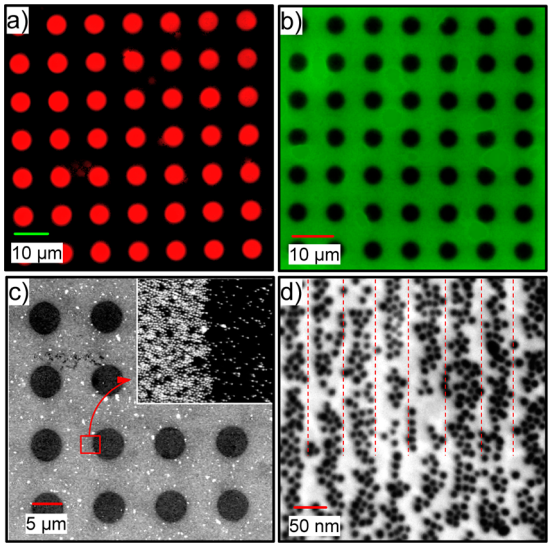

Figure 10. (a,b) FM and (c,d) SEM images of EBL patterned 50 nm PEG films after immersion into (a) a PBS-buffered solution of fluorescently labeled fibrinogen, (b) an aqueous solution of fluorescein, and (c,d) an aqueous solution of citrate-stabilized AuNPs. In a−c, the EBL-generated circulars spots have a diameter of 5 μm, whereas in d, the EBL-generated, AuNP-free stripes have 10 nm nominal width with 50 nm spacing (pristine film), suitable for the adsorption of AuNPs. In all cases, the electron energy and dose were 3 keV and 10 mC/cm^2, respectively. The inset in c shows a part of the image (marked by the red square) with higher magnification. The contrast is inverted in d to get better visualization of the AuNPs.

was adsorbed exclusively on the irradiated areas (bright red spots), while the surrounding PEG matrix remained dark, manifesting the protein-repelling properties of the pristine PEG film.

Alternatively to proteins, patterned PEG films can be immersed into a solution of other molecules, such as a fluorescence dye. As a test compound, we used green fluorescein. After gentle rinsing, the penetration of the dye into the PEG film was examined under a fluorescence microscope (Figure 10b). The absorption of fluorescein results in the reverse pattern as compared to the case of fibrinogen. The irradiated regions appear dark, while the pristine PEG matrix looks bright green. This pattern can be explained by taking into consideration the results of the swelling experiments (see previous section), which imply that water is no longer able to penetrate into the EBL-treated areas. In contrast, the fluorescein was able to penetrate into the pristine PEG areas, getting caught in the matrix (at least to some extent) and staying there even after the rinsing. As for the fibrinogen, it is not clear whether the proteins were not able to penetrate into the PEG matrix under the swelling conditions or they penetrated but, because of the weak interaction with the PEG moieties, were expelled from the matrix along with the buffer solution or during the subsequent rinsing. Note that the above protein adsorption experiments are in agreement with the observed conversion of the hydrophilic PEG films into a deoxygenated, hydrophobic structure upon the irradiation. Poly(ethylene glycols) are considered biocompatible because they are able to bind water molecules.[1] Without this property, proteins can easily adsorb from solution onto the "dry" interface (hydrophilic interactions).

The sealing of the irradiated areas of the PEG films against the penetration of water can also be utilized to create tailored patterns of composite materials. Suitable components in this context are metal nanoparticles, including AuNPs, which we used as the test objects, in particular. Accordingly, a 50 nm PEG film was patterned by EBL as described above, immersed into an aqueous solution of citrate-stabilized AuNPs with a diameter of ∼20 nm, and finally examined with a SEM. Due to the high atomic number of gold, AuNPs are clearly visible in the electron microscope as bright areas. Figure 10c shows the resulting nanocomposite pattern, where the AuNPs are mostly adsorbed into the pristine PEG matrix, whereas the irradiated areas appear noticeably darker. Again, the water and hence the AuNPs were hardly able to penetrate into the areas modified by electrons. At higher magnification, the individual particles became visible as shown in the inset of Figure 10c, and the strong adsorption contrast can be quantified as the adsorption density in terms of the bright−dark ratio. For the pristine PEG films, the ratio is evaluated to be more than 80%, whereas this value for the irradiated sections is lower than 5%. The resolution limit for this novel type of EBL is in the range of several tens of nanometers. Figure 10d shows the SEM image (with inverted contrast) taken after the deposition of AuNPs onto (or into) an array of 5 nm wide lines written with a 50 nm spacing by a focused electron beam in the PEG film. The pattern is not perfect, but the AuNPs stripes are predominantly located within the pristine PEG areas (i.e., between the 5 nm lines) and are clearly separated from one another.

4. CONCLUSIONS

We have studied the modification of nanometer-thin PEG films with electron irradiation and tested the possibility to fabricate different EBL-generated patterns on their basis. The films were prepared by temperature-induced cross-linking of multifunctional, STAR-shaped PEG compounds and offered an excellent model system for the above studies—along with a tunable thickness of 4−100 nm, they possessed high stability, also in aqueous solutions.

Using a combination of XPS and NEXAFS spectroscopy, we demonstrated that electron irradiation results in significant chemical modification and partial desorption of the PEG material. In the course of the irradiation, the initially well-defined PEG films were gradually transformed into carbon-enriched and oxygen-depleted aliphatic films. These films exhibited C−C, C=C, and hydroxy bonding motives with, presumably, a high percentage of intermolecular cross-linking bonds. The modification of the PEG films occurred very rapidly at low doses, slowed down at moderate doses, and demonstrated a leveling off behavior at high doses, following the formation of the irradiation-insensitive, inter-cross-linked aliphatic film.

The severe chemical modification of the PEG films allows the preparation of wettability patterns which, depending on the

length scale of the fabricated features, have, in terms of lithography, either negative or positive character. The significant extent and tunable character of the irradiation-induced desorption makes it possible to sculpt complex 3D micro- and nanostructures from the PEG material on solid supports. The nonirradiated areas of these structures exhibit characteristic swelling behavior typical of PEG hydrogels, while the irradiated areas reveal, depending on the applied dose, either less pronounced swelling behavior or complete inertness to the swelling. The latter areas are, thus, completely sealed to the water penetration, which allows one to prepare nanocomposite patterns based on any object dissolved in water such as fluorophores or metal nanoparticles with a proper organic shell. At the same time, due to the distinct protein-repelling properties of the PEG films, no proteins can be adsorbed into the nonirradiated areas, whereas irradiated areas become prone to the protein adsorption. Thus, the PEG films can be used as a suitable resistance to prepare protein-affinity patterns in a protein-repelling matrix.

The above results suggest that the PEG films of this study as well as, presumably, analogous PEG films prepared by other methods can serve as a versatile platform for EBL-based nanofabrication in different, application-relevant areas of chemistry, biology, and material science.

AUTHOR INFORMATION

Corresponding Author

*Phone: +49(0)6221-54 4921. Fax: +49(0)6221-54 6199. E-mail: Michael.Zharnikov@urz.uni-heidelberg.de.

Notes

The authors declare no competing financial interest.

ACKNOWLEDGMENTS

We thank Thomas Kriesche for the assistance to set up the swelling experiments and the MAX-lab staff, including A. Preobrajenski in particular, for the support during the synchrotron-related measurements. This work has been financially supported by the Volkswagen Stiftung (83227) and DFG (Ec 152/4−1 and ZH 63/9-3).

REFERENCES

(1) Harris, J. M. Biotechnical and Biomedical applications of PEG. In *Poly(ethylene glycol) Chemistry: Biotechnical and Biomedical Applications*; Harris, J. M., Ed.; Plenum Press: New York, 1992; pp 1−12.
(2) Prime, K. L.; Whitesides, G. M. *Science* **1991**, *252*, 1164−1167.
(3) Li, L. Y.; Chen, S. F.; Zheng, J.; Ratner, B. D.; Jiang, S. Y. *J. Phys. Chem. B* **2005**, *109*, 2934−2941.
(4) Christophis, C.; Grunze, M.; Rosenhahn, A. *Phys. Chem. Chem. Phys.* **2010**, *12*, 4498−4504.
(5) Bergstrom, K.; Holmberg, K.; Safranj, A.; Hoffman, A. S.; Edgell, M. J.; Kozlowski, A.; Hovanes, B. A.; Harris, J. M. *J. Biomed. Mater. Res., Part A* **1992**, *26*, 779−790.
(6) Papra, A.; Gadegaard, N.; Larsen, N. B. *Langmuir* **2001**, *17*, 1457−1460.
(7) Malmsten, M.; Emoto, K.; Van Alstine, J. M. *J. Colloid Interface Sci.* **1998**, *202*, 507−517.
(8) Yang, Z. H.; Galloway, J. A.; Yu, H. U. *Langmuir* **1999**, *15*, 8405−8411.
(9) Zdyrko, B.; Klep, V.; Luzinov, I. *Langmuir* **2003**, *19*, 10179−10187.
(10) Groll, J.; Ameringer, T.; Spatz, J. P.; Möller, M. *Langmuir* **2005**, *21*, 1991−1999.
(11) Ma, H. W.; Wells, M.; Beebe, T. P.; Chilkoti, A. *Adv. Funct. Mater.* **2006**, *16*, 640−648.
(12) Larsson, A.; Ekblad, T.; Andersson, O.; Liedberg, B. *Biomacromolecules* **2007**, *8*, 287−295.
(13) Ko, Y. G.; Kim, Y. H.; Park, K. D.; Lee, H. J.; Lee, W. K.; Park, H. D.; Kim, S. H.; Lee, G. S.; Ahn, D. J. *Biomaterials* **2001**, *22*, 2115−2123.
(14) Groll, J.; Fiedler, J.; Engelhard, E.; Ameringer, T.; Tugulu, S.; Klok, H. A.; Brenner, R. E.; Möller, M. *J. Biomed. Mater. Res., Part A* **2005**, *74A*, 607−617.
(15) Meyerbröker, N.; Li, Z. A.; Eck, W.; Zharnikov, M. *Chem. Mater.* **2012**, *24*, 2965−2972.
(16) Ma, H. W.; Li, D. J.; Sheng, X.; Zhao, B.; Chilkoti, A. *Langmuir* **2006**, *22*, 3751−3756.
(17) Chen, R. T.; Marchesan, S.; Evans, R. A.; Styan, K. E.; Such, G. K.; Postma, A.; McLean, K. M.; Muir, B. W.; Caruso, F. *Biomacromolecules* **2012**, *13*, 889−895.
(18) Andreopoulos, F. M.; Beckman, E. J.; Russell, A. J. *Biomaterials* **1998**, *19*, 1343−1352.
(19) Ducker, R. E.; Janusz, S.; Sun, S. Q.; Leggett, G. J. *J. Am. Chem. Soc.* **2007**, *129*, 14842−14843.
(20) Jeyachandran, Y. L.; Terfort, A.; Zharnikov, M. *J. Phys. Chem. C* **2012**, *116*, 9019−9028.
(21) Montague, M.; Ducker, R. E.; Chong, K. S. L.; Manning, R. J.; Rutten, F. J. M.; Davies, M. C.; Leggett, G. J. *Langmuir* **2007**, *23*, 7328−7337.
(22) Ahmad, S. A.; Hucknall, A.; Chilkoti, A.; Leggett, G. J. *Langmuir* **2010**, *26*, 9937−9942.
(23) Ballav, N.; Thomas, H.; Winkler, T.; Terfort, A.; Zharnikov, M. *Angew. Chem., Int. Ed.* **2009**, *48*, 5833−5836.
(24) Ballav, N.; Terfort, A.; Zharnikov, M. *Langmuir* **2009**, *25*, 9189−9196.
(25) Jeyachandran, Y. L.; Zharnikov, M. *J. Phys. Chem. C* **2012**, *116*, 14950−14959.
(26) Jeyachandran, Y. L.; Zharnikov, M. *J. Phys. Chem. C* **2013**, *117*, 2920−2925.
(27) Meyerbröker, N.; Kriesche, T.; Zharnikov, M. *ACS Appl. Mater. Interfaces* **2013**, *5*, 2641−2649.
(28) Moulder, J. F.; Stickle, W. E.; Sobol, P. E.; Bomben, K. D. *Handbook of X-ray Photoelectron Spectroscopy*; Perkin-Elmer Corp.: Eden Prairie, MN, 1992; pp 9−198.
(29) Stöhr, J. *NEXAFS Spectroscopy*; Springer: Berlin, 1992; Vol. 25, pp 276−291.
(30) Batson, P. E. *Phys. Rev. B: Condens. Matter Mater. Phys.* **1993**, *48*, 2608−2610.
(31) Eck, W.; Craig, G.; Sigdel, A.; Ritter, G.; Old, L. J.; Tang, L.; Brennan, M. F.; Allen, P. J.; Mason, M. D. *ACS Nano* **2008**, *2*, 2263−2272.
(32) Ratner, B. D.; Castner, D. G. Electron Spectroscopy for Chemical Analysis. In *Surface Analysis: The Principal Techniques*; Vickerman, J. C., Gilmore, I. S., Eds.; Wiley & Sons: Chichester, U. K., 2009; pp 43−98.
(33) Beamson, G.; Briggs, D. *High Resolution XPS of Organic Polymers*; John Wiley & Sons: Chichester, U. K., 1992; pp 54−275.
(34) Clark, D. T.; Dilks, A.; Thomas, H. R. *J. Polym. Sci., Part A: Polym. Chem* **1978**, *16*, 1461−1474.
(35) Briggs, D.; Seah, M. P. *Practical Surface Analysis by Auger and X-ray Photoelectron Spectroscopy*; John Wiley & Sons: Chichester, U. K., 1990; pp 203−243.
(36) McLafferty, F. W. *Anal. Chem.* **1957**, *29*, 1782−1784.
(37) Zharnikov, M.; Frey, S.; Heister, K.; Grunze, M. *Langmuir* **2000**, *16*, 2697−2705.
(38) Zharnikov, M.; Grunze, M. *J. Vac. Sci. Technol., B* **2002**, *20*, 1793−1807.
(39) Nelson, K. E.; Gamble, L.; Jung, L. S.; Boeckl, M. S.; Naeemi, E.; Golledge, S. L.; Sasaki, T.; Castner, D. G.; Campbell, C. T.; Stayton, P. S. *Langmuir* **2001**, *17*, 2807−2816.
(40) Zwahlen, M.; Herrwerth, S.; Eck, W.; Grunze, M.; Hahner, G. *Langmuir* **2003**, *19*, 9305−9310.
(41) Khan, M. N.; Tjong, V.; Chilkoti, A.; Zharnikov, M. *Angew. Chem., Int. Ed.* **2012**, *51*, 10303−10306.

(42) Meyerbroker, N.; Zharnikov, M. *Langmuir* **2012**, *28*, 9583−9592.
(43) Jeon, S. I.; Andrade, J. D. *J. Colloid Interface Sci.* **1991**, *142*, 159−166.